View Article Online / Journal Homepage / Table of Contents for this issue

Published on 15 October 2009. Downloaded by Michigan State University on 16/01/2016 06:54:04.

This paper is published as part of a *Dalton Transactions* themed issue on:

Thermoelectric Materials

Guest Editor Andrei Shevelkov
Moscow State University, Russia

Published in issue 4, 2010 of *Dalton Transactions*

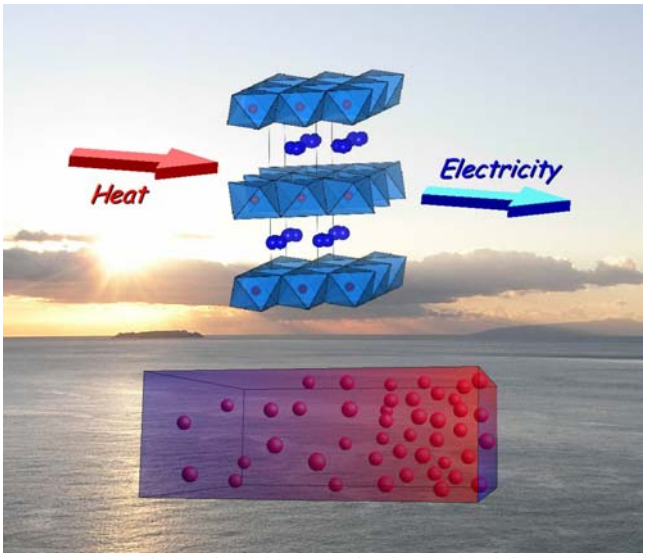

Image reproduced with permission of Ichiro Terasaki

Articles published in this issue include:

PERSPECTIVES:

Thermoelectric clathrates of type I
Mogens Christensen, Simon Johnsen and Bo Brummerstedt Iversen
Dalton Trans., 2010, DOI: 10.1039/b916400f

Wet chemical synthesis and thermoelectric properties of V-VI one- and two-dimensional nanostructures
Genqiang Zhang, Qingxuan Yu and Xiaoguang Li
Dalton Trans., 2010, DOI: 10.1039/b913462j

HOT ARTICLES:

Novel thermoelectric properties of complex transition-metal oxides
Ichiro Terasaki, Manabu Iwakawa, Tomohito Nakano, Akira Tsukuda and Wataru Kobayashi**,**
Dalton Trans., 2010, DOI: 10.1039/b914661j

Effect of Zn doping on improving crystal quality and thermoelectric properties of borosilicides
Takao Mori, David Berthebaud, Toshiyuki Nishimura, Akiko Nomura, Toetsu Shishido and Kazuo Nakajima, *Dalton Trans.,* 2010, DOI: 10.1039/b916028k

Visit the *Dalton Transactions* website for more cutting-edge inorganic and organometallic research
www.rsc.org/dalton

Published on 15 October 2009. Downloaded by Michigan State University on 16/01/2016 06:54:04.

Composition, structure, bonding and thermoelectric properties of "CuT_2P_3" and "CuT_4P_3", members of the $T_{1-x}(CuP_3)_x$ series with T being Si and Ge†

Peng Wang,[a] Faraz Ahmadpour,[a] Taras Kolodiazhnyi,[b] Alfred Kracher,[c] Lachlan M. D. Cranswick[d] and Yurij Mozharivskyj*[a]

Received 20th July 2009, Accepted 15th September 2009
First published as an Advance Article on the web 15th October 2009
DOI: 10.1039/b914555a

Through electron microprobe analysis, X-ray and neutron diffraction, it has been established that "CuT_2P_3" and "CuT_4P_3" (T = Si, Ge) adopt the cubic or tetragonally distorted zinc blende structures in which two element mixtures are present on both atomic sites. One site contains the Cu/T mixture while the other site is occupied by T and P. The structure of "CuT_2P_3" and "CuT_4P_3" can be derived from that of silicon or germanium, in which the single Si or Ge site is broken into two independent sites by the preferential Cu and P substitution. The phases appear to be members of the extended series with a general formula of $T_{1-x}(CuP_3)_x$. The Cu–P ratio of 1 : 3 provides 4 e^- per atom and optimizes the atomic interactions. Thermoelectric performance of "$CuSi_2P_3$", "$CuGe_2P_3$" and "$CuGe_4P_3$" was evaluated from low temperatures to 400 K through resistivity, Seebeck coefficient and thermal conductivity measurements. The Ge-containing phases show a metallic-type behaviour and "$CuSi_2P_3$" is semiconducting with a narrow band gap. The ZT values are bigger for the Ge-containing phases and reach values of 8.49×10^{-3} for "$CuGe_2P_3$" and 1.09×10^{-2} for "$CuGe_4P_3$" at room temperature.

Introduction

Industrial importance of thermoelectric materials lies in their ability to perform cooling/heating when electrical current is applied (Peltier effect) or to generate voltage under a temperature gradient (Seebeck effect).[1] While still suffering from relatively low efficiency, thermoelectric devices offer many advantages over competing technologies in terms of durability, reliability and ease of use. As a result, they find applications in selected fields such as sensors and cooling modules, power generation for remote weather and navigation stations and deep space missions. One of the materials extensively investigated and used for power generation, primarily, for deep-space missions is an (Si, Ge) alloy.[2,3] Its simple structure (diamond-type) and composition (Si and Ge) provide some advantages such as high stability and good Seebeck voltage. But they also carry a few drawbacks such as a high thermal conductivity and a large band gap, which limit their applications to high temperatures, usually above 800 °C. Optimization of thermal conductivity is achieved through the Si/Ge alloying, besides ultrafine particles of silicon nitride or boron nitride are introduced into the (Si, Ge) matrix to disrupt the phonon propagation.[4,5] Still, the large band gap (0.66–1.12 eV depending on the Si/Ge ratio)[6] restricted the material's use to high temperatures.

The (Si, Ge) phases adopt a diamond structure in which tetrahedral bonding around every atom is achieved by having 4 e^- per atom. Similar bonding models are also realized in other semiconductors such as $A^{II}B^{VI}$ and $A^{III}B^{V}$.[6] There are also ternary phases with 4 e^- per atom and tetrahedral bonds, but now elements with a larger range of valences and different ratios can be combined to obtain the same electron count, *e.g.* $A^{II}B^{IV}C_2^{V}$ and $A^{I}B_2^{IV}C_3^{V}$. Among these ternary phases, $CuSi_2P_3$ and $CuGe_2P_3$, discovered back in 1961,[7] were believed to be semiconductors with the bonding features similar to those in the (Si, Ge) alloys. Both $CuSi_2P_3$ and $CuGe_2P_3$ were found to adopt the zinc blende structure with the Cu/Si or Cu/Ge atoms being mixed on one site. It has also been reported that alloying $CuGe_2P_3$ with Ge yields the $CuGe_4P_3$ phase with the same structure as $CuGe_2P_3$.[8] But now in $CuGe_4P_3$, the Cu and P atoms have to be mixed on one site as opposed to the Cu/Ge mixture in $CuGe_2P_3$. Similarly, alloying of $CuSi_2P_3$ with Si has been reported to produce phases with a general formula of $CuSi_{2+x}P_3$ (where x = 1, 2 and 3), but the atomic distribution was not established.[9] All phases regardless of their Si or Ge concentration were found to adopt the cubic zinc blende structure.

The Cu–Si–P and Cu–Ge–P phases may be very attractive in terms of thermoelectric properties as statistical mixtures are likely to reduce their thermal conductivity, and the presence of elements with different electronegativities may decrease the band gap, making these phosphides suitable for power generation at lower temperatures. Through resistivity measurements on a single crystal, $CuSi_2P_3$ was found to have a small band gap of 0.0269(1) eV.[10] Surprisingly, $CuGe_2P_3$ has reported to possess a large band gap of 0.90(5) eV,[11] which could not be substantiated by other literature data.

To understand such unusual variations in physical properties, establish atomic rearrangement and evaluate thermoelectric

[a]*Department of Chemistry, McMaster University, 1280 Main Street West, Hamilton, Ontario, Canada L8S 4M1. E-mail: mozhar@mcmaster.ca*
[b]*National Institute for Materials Science, 1-1 Namiki, Tsukuba, Ibaraki 305-0044, Japan*
[c]*Ames Laboratory, Iowa State University, Ames, Iowa >50011-3020, USA*
[d]*Canadian Neutron Beam Centre, NRC, Chalk River, Ontario, Canada K0J 1J0*

† Electronic supplementary information (ESI) available: Refinement results for "$CuSi_2P_3$" and "$CuGe_2P_3$" from neutron powder diffraction data. Density of states for the binary GeP with the zinc blende structure. See DOI: 10.1039/b914555a

Published on 15 October 2009. Downloaded by Michigan State University on 16/01/2016 06:54:04.

Table 1 Single crystal refinement results for different structural models of "$CuGe_4P_3$" ($F\bar{4}3m$, $a = 5.445(1)$ Å)

Model	$(Cu_{0.95}Ge_{4-0.95})(Ge_{4-x}P_x)$	$Cu_xGe_4P_{4-x}$	$Cu_xGe_{4-x}P_4$
Refined composition	$Cu_{0.95}Ge_{4.48(1)}P_{2.57(1)}$	$Cu_{1.60(8)}Ge_4P_{2.40(8)}$	$Cu_{1.40(8)}Ge_{2.60(8)}P_4$
4*a* site occupancy	Cu/Ge 0.238/0.762	Ge 1.00	Cu/Ge 0.35/0.65(2)
4*c* site occupancy	P/Ge 0.642/0.358(3)	Cu/P 0.40/0.60(2)	P 1.00
R_1 indices	0.0058	0.0168	0.0860
wR_2 indices	0.0120	0.0326	0.2202
Electron density/e Å^{-3}	0.40/−0.13	0.76/−0.48	1.44/−3.08

performance of these phosphides, we undertook a systematic study of their structure, composition and physical properties.

Results and discussion

Composition and site occupancies

The electron microprobe analysis on the hot-pressed $CuSi_2P_3$ sample yielded the $Cu_{1.002(7)}Si_{2.07(2)}P_{2.93(2)}$ composition, which while coming close to the loading composition of $CuSi_2P_3$ deviated significantly from it. A structural model, in which one site is occupied by the Cu/Si mixture and the other only by P atoms, could not be substantiated. The most probable atomic arrangement is the one in which Si is present also on the P site.

For the "$CuGe_2P_3$" and "$CuGe_4P_3$" samples, microprobe data obtained from both the lines scans and random spots yielded the average compositions of $Cu_{0.89(2)}Ge_{2.59(5)}P_{2.52(4)}$ and $Cu_{0.95(2)}Ge_{4.36(8)}P_{2.69(6)}$, respectively. The simple, one-site mixtures of Cu/Ge for $Cu_{0.89(2)}Ge_{2.59(5)}P_{2.52(4)}$ ("$CuGe_2P_3$") and Cu/P for $Cu_{0.95(2)}Ge_{4.36(8)}P_{2.69(6)}$ ("$CuGe_4P_3$") could not be substantiated. Also from the $Cu_{0.95(2)}Ge_{4.36(8)}P_{2.69(6)}$ composition, it can be concluded that germanium has to be present, although in different amounts, on both sites. Additionally, the line scans across the matrix in $CuGe_2P_3$ and $CuGe_4P_3$ revealed significant variations in the composition (Fig. 1) and pointed at a possible peritectic solidification of the main phase along the CuP_3 line and away from Ge. These compositional variations are consistent with the X-ray powder diffraction data. The larger compositional deviations for "$CuGe_4P_3$" as compared to those for "$CuGe_2P_3$" suggest flatter liquidus and solidus surfaces for the Ge-richer sample.

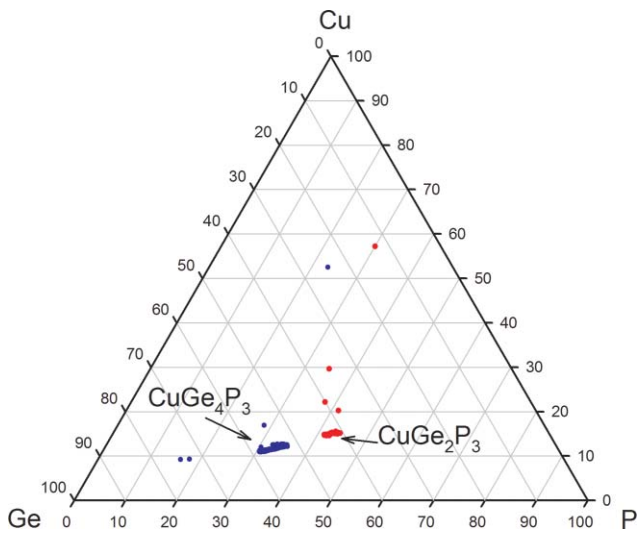

Fig. 1 Composition of the matrixes of the $CuGe_2P_3$ and $CuGe_4P_3$ samples from the line scans.

The microprobe results served as a starting point for the satisfactory refinement of "$CuGe_2P_3$" and "$CuGe_4P_3$" from the single crystal data. Table 1 summarizes the refinement results for the different structural models of "$CuGe_4P_3$". The second column features the model in which the Cu concentration derived from the microprobe analysis was used as reference and Cu/Ge and Ge/P mixtures were assumed on individual sites. The Cu/Ge ratio on the 4*a* site was fixed, while the Ge/P ratio on the 4*c* site was allowed to vary. The resulting composition of $Cu_{0.95}Ge_{4.48(1)}P_{2.57(1)}$ is close to the microprobe composition of $Cu_{0.95(2)}Ge_{4.36(8)}P_{2.69(6)}$, thus validating the proposed structural model. While mixtures of three elements on each site are possible, the X-ray diffraction techniques employed by us cannot differentiate between two and three element mixtures.

A similar approach was used for refining the occupancies in "$CuGe_2P_3$". The resulting composition of $Cu_{0.89}Ge_{2.72(2)}P_{2.39(2)}$ was relatively close to the $Cu_{0.89(2)}Ge_{2.59(5)}P_{2.52(4)}$ formula obtained from the microprobe analysis. Because of the similar X-ray scattering powers of Si and P but different scattering powers of Cu and Si, the P amount was kept constant on one site and the Cu/Si ratio was refined for the other site to yield $Cu_{0.84(3)}Si_{2.16(3)}P_3$ and $Cu_{1.08(3)}Si_{3.92(3)}P_3$ for "$CuSi_2P_3$" and " $CuSi_4P_3$", respectively. The $Cu_{0.84(3)}Si_{2.16(3)}P_3$ formula deviates somewhat more from the microprobe composition of $Cu_{1.002(7)}Si_{2.07(2)}P_{2.93(2)}$ as compared to the similar results for the Ge-containing phases. The refinement results are given in Tables 1 and 2.

Neutron powder diffraction for the $CuSi_2P_3$ and $CuGe_2P_3$ provided an additional check for the proposed structural models. The refined compositions of $Cu_{1.0(4)}Si_{2.0(4)}P_3$ and $Cu_{0.89}Ge_{2.6(2)}P_{2.5(2)}$ are in good agreement with those obtained from the microprobe analysis and the single-crystal X-ray diffraction. Compositions obtained by different techniques are summarized in Table 4.

Structure and boundaries of the $T_{1-x}(CuP_3)_x$ phases

Based on the microprobe and diffraction results, we propose a structural model in which one site is occupied by a Cu/T mixture and the other one by a T/P mixture (T = Si and Ge, Fig. 2). While a three-component mixture on each site cannot be excluded, no unique way to partition the three elements on the two sites can be proposed based on the experimental techniques employed by us. Besides, a significant three-component mixture is unlikely from the chemical prospective. Analysis of the Cu–T, Cu–P and T–P binary phases[12] and binary diagrams[13] indicates that while significant Cu/T and T/P mixtures are found in corresponding binary phases, only a limited substitution of P in the Cu metal (the maximum of 3.5 at% at 700 °C) has been observed.[14] Additionally,

 This journal is © The Royal Society of Chemistry 2010

Published on 15 October 2009. Downloaded by Michigan State University on 16/01/2016 06:54:04.

Table 2 Crystallographic data and structure refinements for single crystals from the $CuSi_2P_3$, $CuGe_2P_3$ and $CuGe_4P_3$ samples at 293 K, MoKα_1 radiation, STOE IPDS II diffractometer

Loading composition	$CuSi_2P_3$	$CuSi_4P_3$	$CuGe_2P_3$	$CuGe_4P_3$
Refined composition	$Cu_{0.84(3)}Si_{2.16(3)}P_3$	$Cu_{1.08(3)}Si_{3.92(3)}P_3$	$Cu_{0.89}Ge_{2.72(2)}P_{2.39(2)}$	$Cu_{0.95}Ge_{4.48(1)}P_{2.57(1)}$
Space group	$I\bar{4}m2$	$F\bar{4}3m$	$F\bar{4}3m$	$F\bar{4}3m$
Lattice parameters/Å	$a = 3.695(1)$ ($\beta = 90°$) $c = 5.225(1)$	$a = 5.241(2)$ —	$a = 5.393(2)$ —	$a = 5.445(1)$ —
V/Å^3	71.35(3)	143.96(8)	156.89(8)	161.44(7)
Z	2/3	1	4/3	1
D_{calcd}/g cm^{-3}	3.205	3.133	4.628	4.784
Crystal size/mm^3	$0.012 \times 0.019 \times 0.022$	$0.044 \times 0.050 \times 0.111$	$0.052 \times 0.090 \times 0.155$	$0.056 \times 0.225 \times 0.251$
2θ range/°	6.76–34.11	6.74–33.99	6.55–33.99	6.49–34.42
Index ranges	$-5 \le h \le 5$ $-5 \le k \le 5$ $-8 \le l \le 8$	$-8 \le h \le 8$ $-8 \le k \le 8$ $-8 \le l \le 8$	$-8 \le h \le 8$ $-8 \le k \le 8$ $-8 \le l \le 8$	$-8 \le h \le 8$ $-8 \le k \le 8$ $-8 \le l \le 8$
Reflections collected	1044	1046	1108	1054
Independent reflections	98 [$R_{int} = 0.0410$]	48 [$R_{int} = 0.0793$]	51 [$R_{int} = 0.0790$]	55 [$R_{int} = 0.0422$]
Completeness to max. 2θ (%)	100	100	100	100
Data/restraints/parameters	98/0/6	48/0/5	51/0/5	55/0/6
GOF on F^2	0.962	0.878	1.149	0.699
Final R indices [$I > 2\sigma(I)$]	$R_1 = 0.0118$, w$R_2 = 0.0187$	$R_1 = 0.0086$, w$R_2 = 0.0150$	$R_1 = 0.0104$, w$R_2 = 0.0248$	$R_1 = 0.0058$, w$R_2 = 0.0120$
R indices (all data)	$R_1 = 0.0173$, w$R_2 = 0.0193$	$R_1 = 0.0110$, w$R_2 = 0.0153$	$R_1 = 0.0104$, w$R_2 = 0.0248$	$R_1 = 0.0058$, w$R_2 = 0.0120$
Absolute structure factor	–0.05(5)	–0.04(4)	0.00	0.00(6)
Extinction coefficient	0	0.10(1)	0.12(1)	0.076(4)
Diffraction peak/hole/e Å^{-3}	0.283/–0.306	0.131/–0.160	0.614/–0.305	0.405/–0.128

Table 3 Atomic and isotropic temperature (U) parameters for $Cu_{0.84(3)}Si_{2.16(3)}P_3$, $Cu_{1.18}Ge_{3.63(3)}P_{3.19(3)}$ and $Cu_{0.95}Ge_{4.48(1)}P_{2.57(1)}$ from single-crystal diffraction data

Atom	Wyckoff symbol	Occupancy	x/a	y/b	z/c	U/Å^2
$Cu_{0.84(3)}Si_{2.16(3)}P_3$ ($CuSi_2P_3$ sample)						
Cu/Si(1)	2*a*	0.28/0.72(1)	0	0	0	0.0046(3)
P(2)	2*d*	1.00	0	1/2	3/4	0.0091(5)
$Cu_{1.08(3)}Si_{3.92(3)}P_3$ ($CuSi_4P_3$)						
Cu/Si(1)	4*a*	0.271/0.729(7)	0	0	0	0.0083(3)
P/Si(2)	4*c*	0.75/0.25	1/4	1/4	1/4	0.0081(4)
$Cu_{1.18}Ge_{3.63(3)}P_{3.19(3)}$ ($CuGe_2P_3$)						
Cu/Ge(1)	4*a*	0.295/0.705	0	0	0	0.0112(3)
P/Ge(2)	4*c*	0.798/0.202(8)	1/4	1/4	1/4	0.0109(5)
$Cu_{0.95}Ge_{4.48(1)}P_{2.57(1)}$ ($CuGe_4P_3$)						
Cu/Ge(1)	4*a*	0.238/0.762	0	0	0	0.0136(1)
P/Ge(2)	4*c*	0.642/0.358(3)	1/4	1/4	1/4	0.0114(2)

Table 4 Composition of the $T_{1-x}(CuP_3)_x$ phases obtained by different techniques

Sample	Electron microprobe	X-Ray single crystal	Neutron powder
$CuSi_2P_3$	$Cu_{1.002(7)}Si_{2.07(2)}P_{2.93(2)}$	$Cu_{0.84(3)}Si_{2.16(3)}P_3$	$Cu_{1.0(4)}Si_{2.0(4)}P_3$
$CuSi_4P_3$	No data	$Cu_{1.08(3)}Si_{3.92(3)}P_3$	No data
$CuGe_2P_3$	$Cu_{0.89(2)}Ge_{2.59(5)}P_{2.52(4)}$	$Cu_{0.89}Ge_{2.72(2)}P_{2.39(2)}$	$Cu_{0.89}Ge_{2.6(2)}P_{2.5(2)}$
$CuGe_4P_3$	$Cu_{0.95(2)}Ge_{4.36(8)}P_{2.69(6)}$	$Cu_{0.95}Ge_{4.48(1)}P_{2.57(1)}$	No data

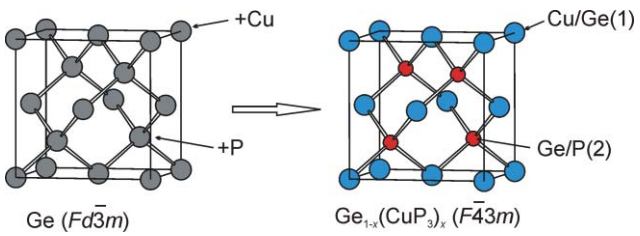

Fig. 2 Relationship between the structures of Ge and $Ge_{1-x}(CuP_3)_x$.

inability to prepare $CuSiP_3$ and $CuGeP_3$, in which P will have to be present on the Cu/T site, precludes existence of substantial three-component mixtures.

According to the proposed model, increase in the T content on going from "CuT_2P_3" to "CuT_4P_3" leads to a bigger population of T on the two sites, while the P : Cu ratio remains close to

Published on 15 October 2009. Downloaded by Michigan State University on 16/01/2016 06:54:04.

3 : 1 (according to the microprobe results, P : Cu = 2.92(3) for "$CuSi_2P_3$", P : Cu = 2.83(6) for "$CuGe_2P_3$" and P : Cu = 2.83(9) for "$CuGe_4P_3$"). The distribution of the elements on the two sites and the ratios between them allow us to view the compounds as members of the extended series with a general formula $T_{1-x}(CuP_3)_x$ (T = Si and Ge). If the series were fully continuous, the end members on the T-rich side would be pure silicon and germanium ($x = 0$), while the other end member would be a binary CuP_3 ($x = 1$), which is unknown. Since $CuSiP_3$ and $CuGeP_3$ could not be prepared under our experimental conditions, the largest value of x has to be smaller than 0.5. Further studies will have to be undertaken to map finer boundaries of the $T_{1-x}(CuP_3)_x$ series.

In terms of atomic arrangements, the $T_{1-x}(CuP_3)_x$ structures could be viewed as derived from the diamond structures of silicon or germanium *via* symmetry reduction and introduction of Cu atoms on one site and P atoms on the other site. While the Ge-containing phases and "$CuSi_4P_3$" keep the cubic zinc blende structure ($F\bar{4}3m$ space group), "$CuSi_2P_3$" adopts a tetragonally distorted version of it ($I\bar{4}m2$). The relationship between the two unit cells can be presented by the following matrix transformation:

$$\begin{pmatrix} 1/2 & 1/2 & 0 \\ -1/2 & 1/2 & 0 \\ 0 & 0 & 1 \end{pmatrix} \begin{pmatrix} \vec{a}_c \\ \vec{b}_c \\ \vec{c}_c \end{pmatrix} = \begin{pmatrix} \vec{a}_t \\ \vec{b}_t \\ \vec{c}_t \end{pmatrix}$$

It is worth noting that the tetragonal distortion disappears as the Si concentration increases. Currently we do not understand the origin of the tetragonal distortion in the Si-containing phases. It has been also reported that tetragonal "$CuSi_2P_3$" prepared through the iodine transport at 800 °C develops a large superstructure easily detectable through the X-ray diffraction.[10] In contrast, the crystals from "$CuSi_2P_3$" prepared by us at 1000 °C show no superstructure reflections even with a large overexposure on the image plate. Additionally, the TEM analysis (not described here) performed by us on the $CuSi_2P_3$ powder indicated no superstructure formation. It can be speculated that the annealing temperature of 1000 °C produces the higher-symmetry lattice, while 800 °C and lower temperatures may yield a lower-symmetry lattice.

Transport properties

Temperature dependence of electrical resistivity, Seebeck coefficient and thermal conductivity is given in Fig. 3–5. Room temperature physical properties for "$CuSi_2P_3$", "$CuGe_2P_3$" and "$CuGe_4P_3$" are summarized in Table 5. The presence of small quantities of Ge and Cu_3P is unlikely to change the values of the Seebeck coefficient and thermal conductivity to a significant extent. We found no published data on the electrical resistivity of Cu_3P. Even assuming the resistivity of Cu_3P to be similar to that of Cu, the resistivity of "$CuGe_2P_3$" and "$CuGe_4P_3$" is underestimated by ~2% (1.15 and 0.80 wt% of Cu_3P, respectively) according to the resistivity-mixture rule for a highly conductive dispersed phase.[15] Since the contribution of Ge to electrical conductivity is opposite to that of Cu_3P, the values given in Table 5 are expected to be close to those for pure phases. There are well-pronounced bumps in the resistivity and only small changes in the Seebeck coefficient around

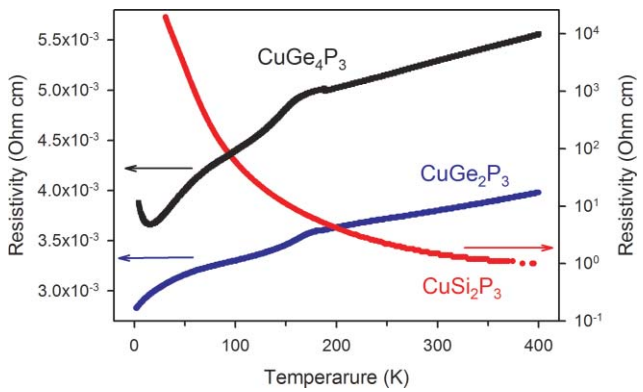

Fig. 3 Electrical resistivity of "$CuSi_2P_3$", "$CuGe_2P_3$" and "$CuGe_4P_3$".

Table 5 Some transport parameters for the $CuSi_2P_3$, $CuGe_2P_3$ and $CuGe_4P_3$ samples at room temperature

Parameter	$CuSi_2P_3$	$CuGe_2P_3$	$CuGe_4P_3$
Resistivity/Ω cm^{-1}	1.50	3.79×10^{-3}	5.28×10^{-3}
Band gap/eV	0.053	0	0
Seebeck coefficient/μV K^{-1}	395	77	96
Thermal conductivity total/W K^{-1} m^{-1}	5.37	5.42	4.71
Electronic thermal conductivity (k_e)/W K^{-1} m^{-1}	4.79×10^{-4}	0.19	0.14
Lattice thermal conductivity (k_l)/W K^{-1} m^{-1}	5.37	5.23	4.57
Figure-of-merit, ZT	5.68×10^{-4}	8.49×10^{-3}	1.09×10^{-2}

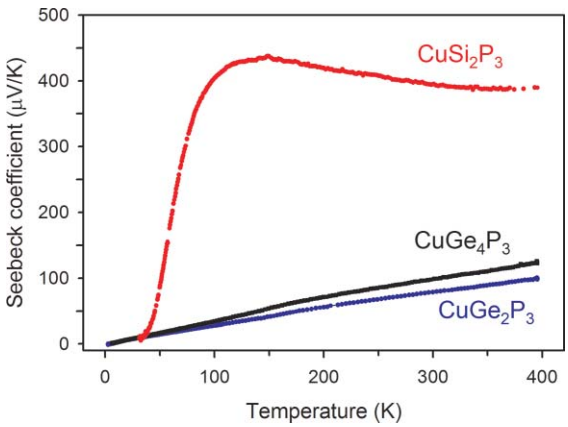

Fig. 4 Seebeck coefficient of "$CuSi_2P_3$", "$CuGe_2P_3$" and "$CuGe_4P_3$".

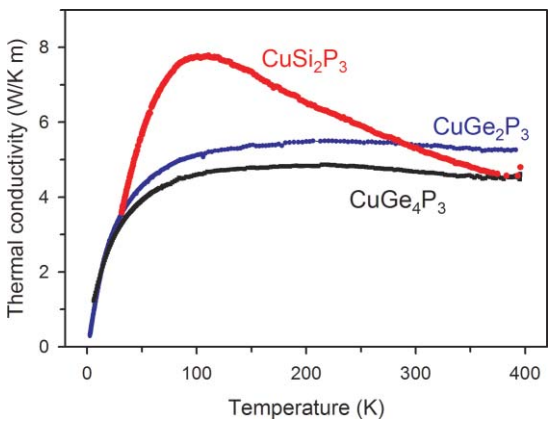

Fig. 5 Thermal conductivity of "$CuSi_2P_3$", "$CuGe_2P_3$" and "$CuGe_4P_3$".

 This journal is © The Royal Society of Chemistry 2010

Published on 15 October 2009. Downloaded by Michigan State University on 16/01/2016 06:54:04.

170–180 K for the both phases. Currently, we cannot explain these features.

The resistivity values obtained by us for the Ge-containing samples are close to those reported by Paplin *et al.* for "$CuGe_2P_3$" ($\rho = 5.9 \times 10^{-3}$ Ohm cm) and "$CuGe_4P_3$" ($\rho = 4.9 \times 10^{-3}$ Ohm cm)[8] but the relationship observed by us between the resistivity and germanium content is reverse. In comparison to the $Si_{1-x}Ge_x$ alloys, "$CuSi_2P_3$", "$CuGe_2P_3$" and "$CuGe_4P_3$" have much lower electrical resistivity than the intrinsic $Si_{1-x}Ge_x$ ($\rho = 10^3$–10^5 Ohm cm for $0.2 < x < 0.85$).[16] However, doped $Si_{1-x}Ge_x$ alloys are more conductive (*e.g.* $\rho = \sim 1.42 \times 10^{-3}$ Ohm cm for the p-type $Si_{0.8}Ge_{0.2}$ +0.5 wt% of B).[17]

The total thermal conductivity of all phases is much lower than the thermal conductivity of pure bulk germanium (58 W K^{-1} m^{-1}) or silicon (130 W K^{-1} m^{-1}) and is also lower than the thermal conductivity of the $Si_{1-x}Ge_x$ alloys (6.28 – 11.74 W K^{-1} m^{-1} for $0.2 < x < 0.85$) at room temperature.[18] Using the Wiedemann–Franz law for degenerate conductors, it is also possible to calculate the electronic part of the thermal conductivity ($k_e = LT/\rho$, with L being the Lorenz number) and subsequently the lattice thermal conductivity, k_l.[19] While "$CuGe_2P_3$" and "$CuGe_4P_3$" can be considered as degenerate conductors (heavily-doped degenerate semi-conductors), "$CuSi_2P_3$" is likely to behave as a non-degenerate semi-conductor for which the Lorenz number is a function of an exponent, λ, that is usually unknown.[20] Still, treating "$CuSi_2P_3$" as a degenerate conductor will not alter the lattice contribution significantly. It is found that in all phases the electronic contribution is relatively low and the lattice contribution dominates the thermal conductivity.

The dimensionless figure-of-merit, ZT, as a function of temperature for three materials is given in Fig. 6. The ZT value is bigger for the Ge-containing phases due to their lower electrical resistivity, with "$CuGe_4P_3$" having the highest ZT. Although the room temperature ZT values are relatively low, the steep upward trend suggests that much higher values can be achieved at elevated temperatures. Future studies on these phases will explore their transport properties above room temperature.

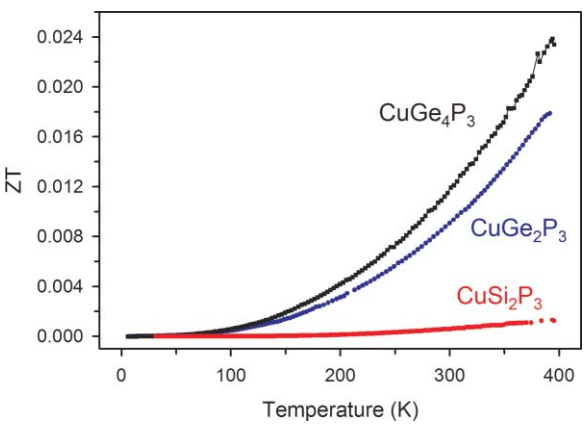

Fig. 6 Dimensionless figure-of-merit, ZT, as a function of temperature for "$CuSi_2P_3$", "$CuGe_2P_3$" and "$CuGe_4P_3$".

Electronic structure of $CuSi_4P_3$ and $CuGe_4P_3$

Electronic structure calculations were performed to understand bonding features, stoichiometry and electrical conductivity of the "CuT_2P_3" and "CuT_4P_3" phases. Calculated density of states, DOS, (Fig. 7) for the hypothetical, ordered structures of $CuSi_4P_3$ and $CuGe_4P_3$ are quite similar with one feature being significantly distinct: presence of a small band gap of 0.04 eV in $CuSi_4P_3$ and its closure in $CuGe_4P_3$. Such difference can be related to the stronger bonding involving the Si orbitals, which brings down the bonding states and pushes up the antibonding states, thus, opening the band gap. Similar densities of states can be assumed for "$CuSi_2P_3$" and "$CuGe_2P_3$". While the DOS calculations agree reasonably well with the electrical resistivity measurements that yielded a small band gap of 0.053 eV for the "$CuSi_2P_3$" phase (Table 5) and metallic-type behaviour for the Ge-containing ones, the calculations do not account for the statistical mixtures that are likely to influence the electrical resistivity. Nevertheless, the claim by Berger *et al.* that "$CuGe_2P_3$" has a band gap of 0.90(5) eV[11] could neither be substantiated by our calculations nor by the resistivity measurements.

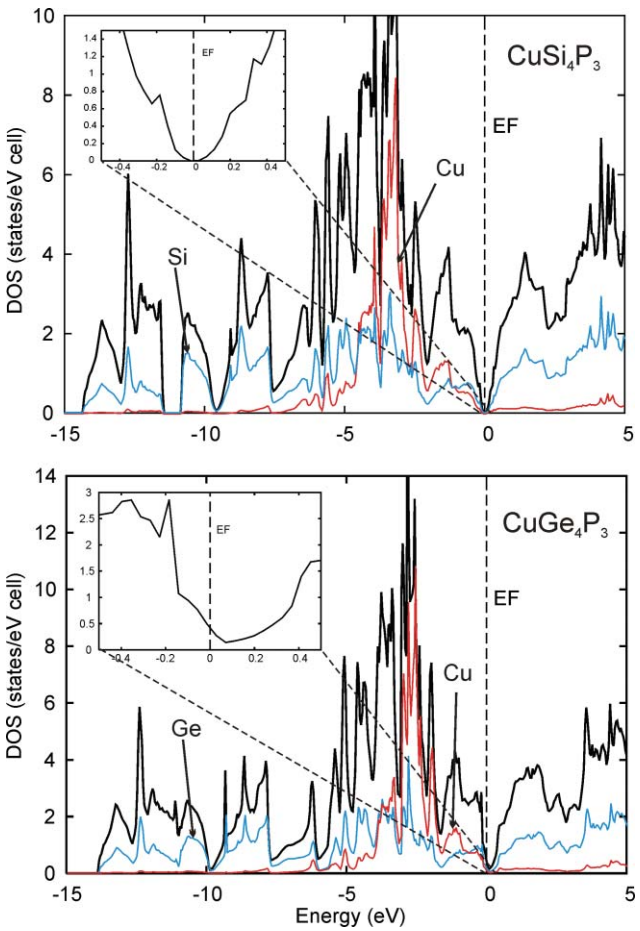

Fig. 7 Calculated densities of states (DOS) for ordered $CuSi_4P_3$ and $CuGe_4P_3$.

It is interesting to understand the reasons for the band gap contraction in $CuSi_4P_3$ and closure in $CuGe_4P_3$ as compared to pure Si and Ge. The calculation performed for the high-pressure modification of GeP with the zinc blende structure[21] reveal a band gap of ~1 eV for the electron count of 4 e^- per atom (see ESI†). While the Ge : P ratio in $CuGe_4P_3$ is different from being equiatomic as in GeP, it is unlikely that a different Ge : P ratio

Published on 15 October 2009. Downloaded by Michigan State University on 16/01/2016 06:54:04.

leads to the closure of the band gap. A substantial contribution of the Cu states, primarily from the d orbitals, just below the Fermi level indicates that the Cu atoms are responsible for the metallic behaviour. Similar arguments can be applied to explain the DOS features of $CuSi_4P_3$.

The tetrahedral environment around each atom in $CuSi_4P_3$ and $CuGe_4P_3$ and the 4 e^- per atom count are expected to result in the scenario where all the bonding states are populated and antibonding states are empty. The calculated COHP curves for $CuGe_4P_3$ between Cu1, Ge1 atoms and the site 2 atoms prove that the interactions are indeed optimized for the 4 e^- per atom count (Fig. 8). Thus, significant deviations from the Cu : 3P ratio is energetically unfavourable as a lower electron count diminishes bonding interactions whereas a larger electron count results in the population of antibonding states. The lower limit for the Cu : 3P ratio is likely to be around 2.8, as both Ge-phases are found to have this ratio (Cu : P = 2.83(6) for "$CuGe_2P_3$", Cu : P = 2.83(9) for "$CuGe_4P_3$" and Cu : P = 2.91(3) for "$CuSi_2P_3$"). Such Cu : P ratios yield a lower than 4 e^- per atom count and render the phases p-type conductors (in agreement with the Seebeck coefficient).

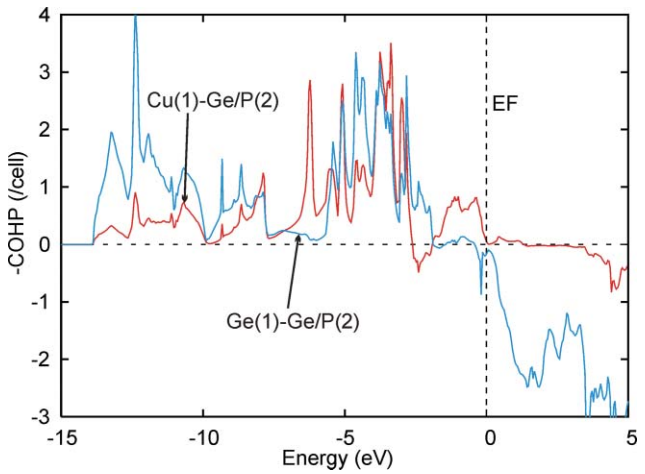

Fig. 8 Crystal orbital Hamilton population (COHP) for selected interactions in $CuGe_4P_3$.

Experimental

Synthesis

The starting materials were pieces of Cu (99.9 wt%, Alfar Aesar), Si (99.999 wt%, Alfa Aesar), Ge (99.999 wt%, Alfa Aesar) and a powder of amorphous red phosphorus (99.5 wt%, Cerac Inc.). The copper and silicon or germanium with either 1 : 1, 1 : 2 or 1 : 4 ratios were arc-melted in the argon atmosphere, ground, mixed with the corresponding phosphorus amount to yield CuT_xP_3 (T = Si, Ge, x = 1, 2 and 4) compositions with a total sample mass of 5 g. The samples were sealed in the evacuated silica tubes 15 cm in length, heated at 4 °C h^{-1} for the Si-containing and 50 °C h^{-1} for the Ge-containing samples to the target temperatures of 800, 900 or 1000 °C, kept at that temperature from 12 to 72 h and water-cooled. Regardless of the annealing temperature and time, the $CuSiP_3$ and $CuGeP_3$ phases could not be obtained. Also, all samples contained some unreacted phosphorus. To remove white phosphorus condensed from vapours, the tube end containing the sample was heated to 400 °C in a horizontal tube furnace while the other end was cooled by a wet towel. After the white phosphorus had re-condensed at the cold end, the tube was removed from the furnace and air-cooled.

The Si-containing samples were always solids (powders) at the annealing temperatures, and the Ge-containing ones were liquids at and above 800 °C. While none of the heat treatments could yield 100% pure samples, annealing at 1000 °C for 72 h was found to produce the most homogeneous samples with the lowest amount of impurities and, thus, was chosen as a synthetic route. Still, the $CuSi_4P_3$ sample annealed at 1000 °C contained large quantities of Cu_3Si (Table 1). Interestingly, the Ge-containing samples showed significant compositional variations as discussed above.

Hot pressing

The $CuSi_2P_3$ and $CuSi_4P_3$ samples were powders and required hot pressing for microprobe analysis and physical property measurements. Since the $CuSi_4P_3$ sample contained a significant amount of Cu_3Si, we have proceeded with the $CuSi_2P_3$ sample only. The $CuSi_2P_3$ powder was ground and pre-pressed in a 12 mm graphite die in the argon-filled glove box. The die was transferred in the sealed container to the hot press, where the samples were annealed at 1073 K for 2 h under the pressure of 1 metric ton in an argon atmosphere.

Microprobe analysis

Quantitative electron probe microanalysis was performed on the air-cooled $CuSi_2P_3$, $CuGe_2P_3$ and $CuGe_4P_3$ samples employing a JEOL JXA-8200 Superprobe with 20 kV acceleration potential and 20 nA beam current. Pure elements were used as standards for Si, Ge and Cu. Crystals of CuP_2 grown through an iodine transport were used as standard for P. The composition of CuP_2 crystals was verified from the single-crystal X-ray diffraction data collected on a STOE IPDSII diffractometer. Copper was also calibrated on the CuP_2 standard, and results were found to be identical within analytical uncertainty to calibrating on Cu metal.

The 4th order CuKα line (4λ = 6.1674 Å) overlaps the P Kα line used for the analysis of P (λ = 6.1589 Å), and a linear correction was applied to account for this interference. The correction amounts to 0.2% of the P signal for a Cu : P ratio of 1 : 3. For a single data point this is within analytical uncertainty, but it becomes statistically significant for aggregate data.

X-Ray powder and single-crystal diffraction

X-Ray powder diffraction profiles in the 20–100° 2θ range were recorded on a PANalytical X'Pert Pro diffractometer with an X'Celerator detector and a $CuK_{\alpha 1}$ radiation. The full-profile Rietveld refinement (Rietica program[22]) was used to obtain the lattice constants and to determine impurity concentrations (Table 6). It was found that "$CuGe_2P_3$", "$CuGe_4P_3$" and "$CuSi_4P_3$" adopt the cubic zinc-blende structure (space group, $F\bar{4}3m$) while "$CuSi_2P_3$" is tetragonally distorted (space group $I\bar{4}m2$, Fig. 9).

The air-cooled $CuGe_2P_3$ sample showed slight peak broadening, and $CuGe_4P_3$ exhibited closely spaced peaks that could be associated at least with three phases (Fig. 10). Lattice constants of "individual" components of "$CuGe_4P_3$" could not be reliably refined because of the peak overlap. Compositional inhomogeneity

 This journal is © The Royal Society of Chemistry 2010

Published on 15 October 2009. Downloaded by Michigan State University on 16/01/2016 06:54:04.

Table 6 Lattice constants and impurity levels from powder diffraction for the samples annealed at 1000 °C for 72 h followed by air-cooling

Sample	Major phase	Space group	Lattice constants/Å	Impurities and amounts (wt%)
$CuSi_2P_3$	"$CuSi_2P_3$"	$I\bar{4}m2$	$a = 3.70724(3)$ $c = 5.19471(5)$	Cu_3P 0.19(2)%, Si 2.08(4)%
$CuSi_4P_3$	"$CuSi_4P_3$"	$F\bar{4}3m$	$a = 5.24811(6)$	Cu_3Si 12.8(3)%
$CuGe_2P_3$	"$CuGe_2P_3$"	$F\bar{4}3m$	$a = 5.39598(2)$	Cu_3P 1.15(2)%, Ge 1.67(2)%
$CuGe_4P_3$	"$CuGe_4P_3$"	$F\bar{4}3m$	$a =$ 5.454–5.441	Cu_3P 0.80(2)%, Ge 1.99(3)%

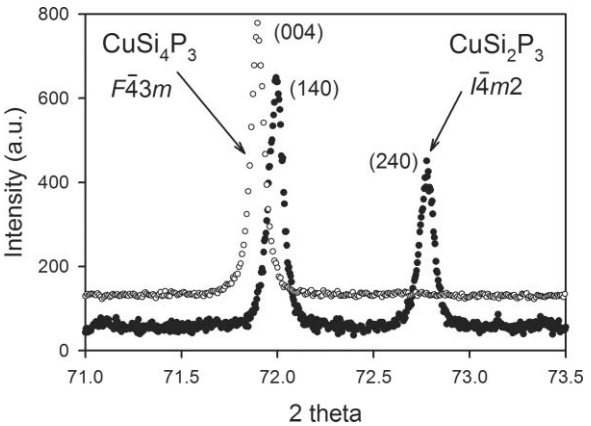

Fig. 9 Peak splitting in "$CuSi_2P_3$" as compared to "$CuSi_4P_3$" indicates the tetragonal distortion.

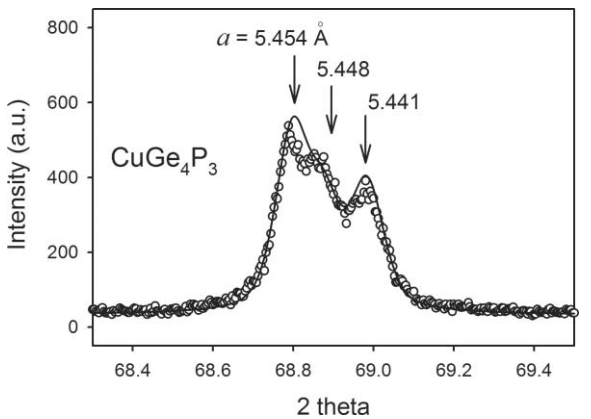

Fig. 10 Experimental (dots) and fitted (solid line) profiles for the $CuGe_4P_3$ sample. Three components with different lattice constants are assumed.

obtained from the X-ray analysis for "$CuGe_2P_3$" and "$CuGe_4P_3$" was consistent with the compositional variations observed during the electron microprobe analysis.

Single-crystal X-ray diffraction data were collected on a STOE IPDSII diffractometer with the MoKα radiation in the whole reciprocal sphere. A numerical absorption correction was based on the crystal shape that was originally derived from the optical face indexing but later optimized against equivalent reflections using STOE X-Shape software.[23] Structural refinement was performed using the SHELXL program (Table 2–3).[24] Further details of the crystal structure investigations can be obtained from the Fachinformationszentrum Karlsruhe, 76344 Eggenstein-Leopoldshafen, Germany, (fax: (49) 7247-808-666; e-mail: crysdata@fiz.karlsruhe.de) on quoting the depository CSD numbers 419641 for $Cu_{0.84(3)}Si_{2.16(3)}P_3$, 419643 for $Cu_{1.08(3)}Si_{3.92(3)}P_3$, 419644 for $Cu_{0.89}Ge_{2.72(2)}P_{2.39(2)}$ and 419642 for $Cu_{0.95}Ge_{4.48(1)}P_{2.57(1)}$.

Neutron powder diffraction

The room temperature neutron data for the air-cooled $CuSi_2P_3$ and $CuGe_2P_3$ samples were collected on the NRC's C2 powder neutron diffractometer at Chalk River, Ontario, Canada. C2 consists of a curved 800 wire position sensitive detector covering a range of 80° with angular wire spacing of 0.1002425°. Further details of the C2 diffractometer can be found in Ref. 25 and 26. The powder diffraction pattern for the $CuSi_2P_3$ and $CuGe_2P_3$ samples were taken in a vanadium sample can over the 2θ range of 38–114° with a wavelength of $\lambda = 1.33037$ Å. The atomic parameters obtained from the corresponding single crystal refinements were used as starting models for the full-profile Rietveld refinements (Rietica program,[22] Fig. 11). The same refinement approaches as for the X-ray single crystal data were used for the neutron data. The refinement results are provided in the ESI.†

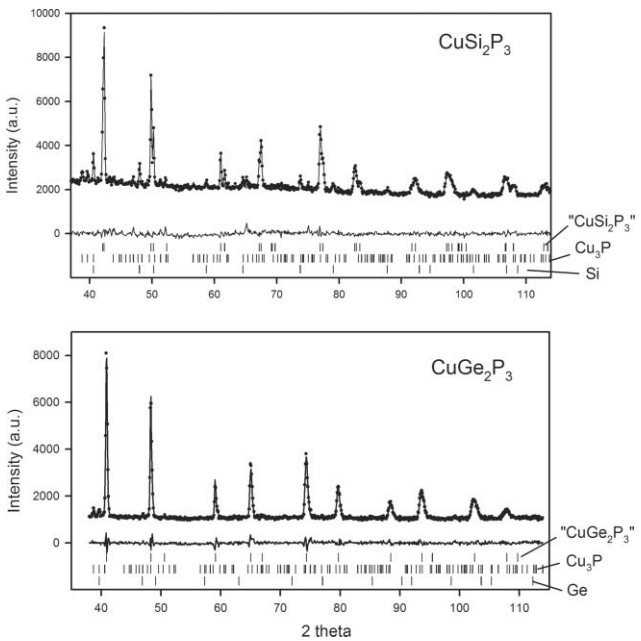

Fig. 11 Rietveld refinements for "$CuSi_2P_3$" and "$CuGe_2P_3$" from the neutron data. Dots and two solid lines represent observed and calculated profiles and the difference between them, respectively. Vertical bars show positions of Bragg peaks.

Physical property measurements

The electrical resistivity, Seebeck voltage and thermal conductivity of "$CuSi_2P_3$", "$CuGe_2P_3$" and "$CuGe_4P_3$" were measured in the 2–400 K (30–400 K for "$CuSi_2P_3$") region on a QD PPMS instrument. The thermal conductivity was measured using the two-probe configuration of the Thermal Transport Option (TTO) of the QD PPMS. The data were collected in the continuous

Published on 15 October 2009. Downloaded by Michigan State University on 16/01/2016 06:54:04.

measurement mode at a cooling rate of 0.2 K min^{-1}. The power and period of the heating pulses were automatically adjusted to create a thermal gradient across the sample of 3% of the ambient temperature. Thermal conductivity was obtained by fitting the time–temperature dependencies of the hot and cold thermometers by the TTO software assuming that the infrared emissivity of the polycrystalline samples is close to 1. Thermally evaporated Al contacts have been used as contact pads for four-probe electrical resistivity measurements. Spring-loaded rhodium-plated Be-Cu pin contacts have been utilized to ensure excellent mechanical and electrical contact with the sample during electrical resistivity measurements. The band gap of 0.053 eV for "$CuSi_2P_3$" was determined from the Arrhenius behaviour of the resistivity in the high temperature region assuming one type of charge carriers.

Electronic structure calculations

Tight-binding linear-muffin-tin-orbital calculations using the atomic sphere approximation (TB-LMTO-ASA)[27] were carried out for an idealized $CuSi_4P_3$ and $CuGe_4P_3$ structures with the lattice constants of the corresponding single crystals. The symmetry was reduced to trigonal to allow the following atomic arrangement: 1 Cu atom at 0 0 0; 3 Si/Ge atoms at $\frac{1}{2}$ 0 $\frac{1}{2}$, $\frac{1}{2}$ $\frac{1}{2}$ 0, 0 $\frac{1}{2}$ $\frac{1}{2}$; 1 Si/Ge atom at $\frac{1}{4}$ $\frac{1}{4}$ $\frac{1}{4}$ and 3 P atoms at $\frac{1}{4}$ $\frac{3}{4}$ $\frac{3}{4}$, $\frac{3}{4}$ $\frac{1}{4}$ $\frac{3}{4}$, $\frac{3}{4}$ $\frac{3}{4}$ $\frac{1}{4}$. To satisfy the overlap criteria of the atomic spheres in the TB-LMTO-ASA method, empty spheres were included into the unit cell. A tetrahedron integration method was used with a total of 512 points in the irreducible wedge of the Brillouin zone. For comparison, the electronic structure of the GeP binary with the cubic zinc blende structure[21] has been also calculated.

Conclusion

The "CuT_2P_3" and "CuT_4P_3" phases (T = Si, Ge) with the zinc blende structure appear to be members of the extended $T_{1-x}(CuP_3)_x$ series, in which two-element mixtures, Cu/T and T/P, are present on both atomic sites. The large statistical mixtures significantly reduce the thermal conductivity of "CuT_2P_3" and "CuT_4P_3" as compared to pure Si and Ge. However, the thermal conductivity is still relatively large, which in combination with low electrical conductivity does not allow to reach desirable ZT values at room temperature. The Ge-containing phases show metallic-type behaviour while "$CuSi_2P_3$" is semiconducting with $\Delta E = 0.053$ eV. Reduction or closure of the band gap in the ternary phases as compared to Si or Ge is caused primarily by the Cu d-states.

Acknowledgements

This work was supported by a Discovery Grant from the Natural Sciences and Engineering Research Council of Canada and by a grant from the ACS Petroleum Research Fund.

References

1 T. M. Tritt, *Science*, 1996, **272**, 1276.
2 D. T. Morgan, *Proc. Int. Power Sources Symp.*, 1986, 76.
3 J. F. Braun and R. J. Hemler, *Proc. Symp. Space Nucl. Power Syst., 7th*, 1990, **2**, 794.
4 J. S. Beaty, J. L. Rolfe, J. Vandersande and J. P. Fleurial, *AIP Conf. Proc.*, 1992, 332.
5 N. Scoville, C. Bajgar, J. Rolfe, J. P. Fleurial and J. Vandersande, *Proceedings of the Intersociety Energy Conversion Engineering Conference*, 1993, **28th**, 1227.
6 R. A. Smith, *'Semiconductors. 2nd Ed'*, Cambridge University Press, 1978.
7 O. G. Folberth and H. Pfister, *Acta Crystallogr.*, 1961, **14**, 325.
8 B. R. Pamplin and M. S. Osmar, *Progress in Crystal Growth and Characterization*, 1984, **10**, 183.
9 G. Bhikshamaiah, M. S. Omar and S. V. Suryanarayana, *Cryst. Res. Technol.*, 1994, **29**, 277.
10 Y. Mozharivskyj, O. Lang and H. F. Franzen, *Z. Anorg. Allg. Chem.*, 2000, **626**, 2153.
11 L. I. Berger, V. I. Sokolova and V. M. Petrov, *Trudy IREA*, 1967, **30**, 406.
12 P. Villars, and L. D. Calvert, in *'Pearson's Handbook of Crystallographic Data for Intermetallic Phases'*, Materials Park, Ohio, 1991.
13 T. B. Massalski, H. Okamoto, P. R. Subramanian, and L. Kacprzak, in *'Binary Alloy Phase Diagrams'*, Materials Park, Ohio, 1990.
14 D. K. Crampton, H. L. Burghoff and J. T. Stacy, *Am. Inst. Mining Met. Engrs., Inst. Metals Div., Tech. Pub.*, 1940, **No. 1142**, 17.
15 S. O. Kasap, *'Principles of Electronic Materials and Devices'*, McGraw-Hill, 2006.
16 G. Busch and O. Vogt, *Helv. Phys. Acta*, 1960, **33**, 437.
17 S. Hwang, W. Min, I. Park, Y. Park, Y. Kim and Y. Park, *Mater. Sci. Forum*, 2007, **544–545**, 745.
18 F. Schaffler, in *'Silicon-germanium (Si1-xGex)'*, ed. M. E. Levinshtein, S. L. Rumyantsev, and M. S. Shur, New York, 2001.
19 R. D. Barnard, *'Thermoelectricity in Metals and Alloys'*, Taylor & Francis Ltd., 1972.
20 H. J. Goldsmid, *'Thermoelectric Refrigeration'*, Plenum Press, 1964.
21 J. Osugi, R. Namikawa and Y. Tanaka, *Rev. Phys. Chem. Japan*, 1967, **37**, 81.
22 B. A. Hunter, and C. J. Howard, in *'Rietica'*, Menai, Austalia, 2000.
23 STOE & Cie GmbH, *X-SHAPE Version 2.05 and X-RED32 Version 1.10*, Darmstadt, Germany, 2004.
24 G. M. Sheldrick, *SHELXL97 and SHELXS97*, University of Gottingen, Germany, 1997.
25 M. Potter, H. Fritzsche, D. H. Ryan and L. M. D. Cranswick, *J. Appl. Crystallogr.*, 2007, **40**, 489.
26 L. M. D. Cranswick, R. Donaberger, I. P. Swainson and Z. Tun, *J. Appl. Crystallogr.*, 2008, **41**, 373.
27 O. K. Andersen, Z. Pawlowska and O. Jepsen, *Phys. Rev. B: Condens. Matter Mater. Phys.*, 1986, **34**, 5253.

 This journal is © The Royal Society of Chemistry 2010